In situ monitoring of the martensitic transformation induced by plasticity in a stainless steel

Wajih Jbara[a], Alain Koster[a], Matthieu Rambaudon[a], Laurent Daniel[b,c], Antoine Debray[a], Mathieu Domenjoud[b,c], Yann Le Bihan[b,c], Jean-Claude Le Flour[d], Lucas Sannier[d], Florian Loubeau[d], Yves Bienvenu[a], Vincent Maurel[a,1]

[a]*MINES Paris - PSL, MAT - Centre des Matériaux, CNRS UMR 7633, 21 Allée des Marronniers, 78000 Versailles, France*
[b]*Université Paris-Saclay, CentraleSupélec, CNRS, Laboratoire de Génie Electrique et Electronique de Paris, 91192 Gif-sur-Yvette, France*
[c]*Sorbonne Université, CNRS, Laboratoire de Génie Electrique et Electronique de Paris, 75252 Paris, France*
[d]*RENAULT*

Abstract

Background: The current understanding of strain-induced martensitic transformation in AISI 304L stainless steel lacks comprehensive non-destructive testing (NDT) for effective monitoring, limiting the ability to assess phase transformation in industrial applications. **Objective:** This study aims to develop and evaluate NDT methods for monitoring strain-induced martensitic transformation in AISI 304L stainless steel. **Methods:** The research employs direct microscopic analyses, including optical microscopy and electron backscatter diffraction (EBSD), alongside indirect NDT techniques such as microhardness testing, magnetic permeability measurements, and eddy current (EC) sensor inductance evaluations. Novel aspects include the integration of these methods to correlate phase transformation with measurable properties. **Results:** The study finds that the martensitic phase fraction increases significantly beyond 25 % strain, with inductance and permeability showing strong correlations with phase transformation. Tensile and equibiaxial tests indicate that inductance measurement is a promising tool for monitoring transformations in complex geometries, while microhardness reflects material hardening but lacks direct correlation with phase transformation. **Conclusions:** The findings support EC sensor measurements as a robust method for NDT applications in assessing strain-induced transformations in stainless steel from lab specimens to complex components.

Keywords: Digital image correlation (DIC); Magnetic permeability; Eddy current testing; Martensitic phase transformation.

All authors have no conflicts of interest.

Contents

*Corresponding author. Vincent Maurel, E-mail address: vincent.maurel@minesparis.psl.eu

1. Introduction

Austenitic stainless steel (SS) is the material of choice for the non-magnetic parts of electric motors. It can be used for the stator housing or in other components of electrical equipment for high power units such as those promoted in modern automobiles [1, 2]. However, for some compositions of steel designed for high temperature applications, a martensitic transformation can occur under high stress, such as that associated with die casting [3]. The magnetic properties associated with the martensitic phase can increase the magnetic losses of the electrical device. This issue has been the subject of intensive studies to correlate uniaxial strain with the martensite phase fraction by microscopic analysis. The main effects that have been demonstrated are a drastic sensitivity to alloy composition, temperature and strain rate [4, 5].

Fewer studies deal with the effect of multiaxial loading, and again, depending on the alloy composition and strain rate, the phase transformation could be either increased or decreased for multiaxial loading. For 304 SS, Shin *et al.* [6] observed increased transformation in shear as compared to tension using equal channel angular pressing set-up, whereas for 301 SS, shear could yield to lower phase transformation as compared to other loadings [7, 8]. In addition, multiaxial loading calls for an equivalent strain criterion to describe the effect of multiaxiality. For example, instead of maximum principal strain, von Mises equivalent strain gives a similar phase fraction for 304 SS when comparing tensile testing and flat-punch testing considered as equibiaxial loading [4]. However, other authors have demonstrated the critical influence of the Lode parameter in the phase transformation [9–11]. The martensitic transformation occurs on crystallographic planes of optimal orientation with respect to the loading [12–15]. Considering a SS as a polycrystal aggregate, this means that under multiaxial loading more grains could show an orientation promoting martensitic transformation. As observed for twinning, multiple localisations could either increase or decrease the transformation rate [16]. In addition, martensitic transformation shows a threshold effect at the onset of phase transformation [17]. Again, this threshold is sensitive to compositional effects and multiaxial loading. From neutron diffraction, it is observed that this threshold value drops from 26 to 15 % when considering uniaxial and equibiaxial loading respectively [15].

The measurement of martensitic phase transformation is also a crucial point. First, due to the strong influence of the martensitic phase on magnetic and mechanical properties [9, 18], precise detection of martensitic phase transformation is required. Second, there is a need for in situ measurements in order to detect phase transformation in complex industrial parts in a non destructive way [19]. The most popular approach is based on the measurement of magnetic permeability and saturation magnetisation using magnetometric equipment or the so-called Feritscope [12, 20, 21]. However, the calibration of the measurement still raises practical issues [17]. Among magnetometric techniques, the fluxmetric approach [22], where a magnetic flux is generated by excitation coils wounded around a magnetic circuit, could be used to obtain a full magnetic behavior characterization. These setups ensure accurate and reliable measurements without the need for calibration procedures. However, their limitations stem from the geometry of the specimens, which is influenced by the configuration of the excitation system. Consequently, the technique is not well-suited for in situ measurements. Besides, the strain within the specimen to be measured magnetically should be as homogeneous as possible, to limit uncertainties in the correlation between strain and magnetic properties, because the magnetic measurement is global (averaged over the specimen).

Another technique of interest consists in the use of eddy current (EC) non-destructive testing (NDT). The EC sensor consists of a coil fed by a low intensity alternating current and placed in the vicinity of the target medium. The magnetic field created by the coil is modified by the target as a function of its electrical conductivity and magnetic permeability. This in turn leads to a dependence of the sensor impedance on the electromagnetic properties of the target [23, 24].

This paper aims to calibrate non-destructive testing measurements to assess phase transformation in AISI 304 L alloy. The paper describes mechanical testing under uniaxial loading using digital image correlation (DIC). The subsequent measurements of phase transformation are performed using microscopic analysis by optical microscopy (OM) and electron back scatter diffraction (EBSD) technique. Then, non-destructive testing methods, including the standard Vickers hardness (HV), magnetic permeability and EC sensor technique are implemented. Both mechanical behavior and phase transformation are identified for uniaxial loading. It is shown that the various approaches provide consistent results. The EC sensor technique is finally applied in the case of equibiaxial plastic loading to assess the level of martensitic phase transformation, which serves as a validation case for the proposed methodology. The flowchart of the analysis is detailed in Figure 1.

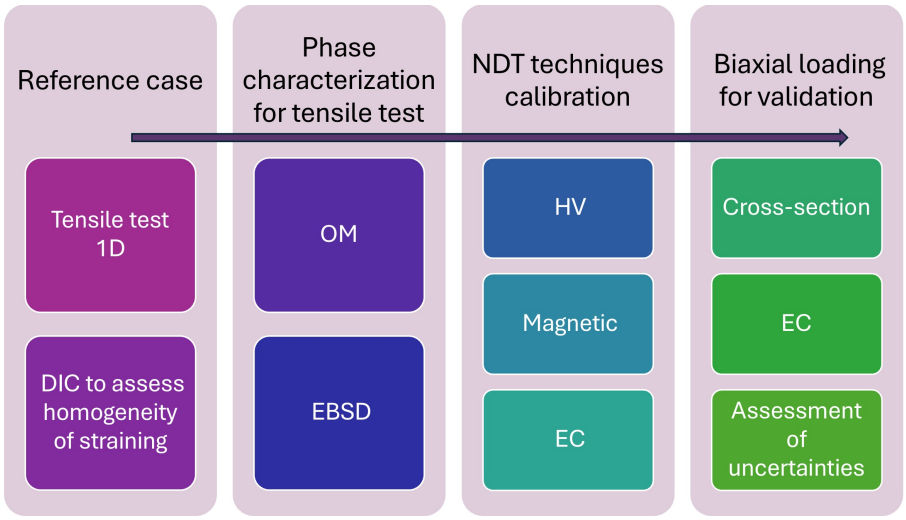

Figure 1: Flowchart summarizing different steps of the proposed analysis.

2. Mechanical characterization under tensile stress of AISI 304L

2.1. Material

The studied material is the AISI 304L stainless steel, processed in sheet of 3 mm by successive steps of hot and cold rolling. The composition of the alloy corresponds to its standard range, Table 1.

Table 1: Chemical composition of AISI 304/1.4307 alloy (wt %).

C	Si	Mn	P	S	N	Cr	Ni	Fe
≤ 0.07	$\leq 1.$	$\leq 2.$	0.045	≤ 0.015	≤ 0.11	17.5-19.5	8.-10.5	Bal.

2.2. Tensile tests

Tensile specimens are processed by electro-discharge machining (EDM), with surface polishing but no further modification of the edge of the sample after EDM. The shape of the sample corresponds to the sketch in Figure 2.

To assess the influence of rolling on the induced anisotropy, the testing methodology was applied in both rolling (RD) and transverse (TD) direction. A speckle was painted on the surface of the sample and strain field measurements were achieved using digital image correlation (DIC) technique [25]. The spatial resolution is about 2.5 mm.

The mechanical behavior is very similar for RD and TD, the yield stress being slightly lower for RD compared to TD samples, and ultimate stress being equal. The average strain to failure was about 52 % and 57 % for RD and TD respectively, Figure 3a.

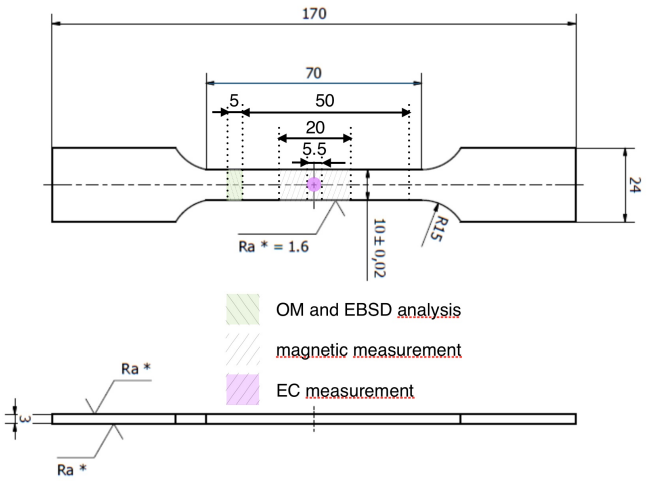

Figure 2: Sample geometry (dimensions in mm), and detailed areas used for the analyses: the central area of 5.5 mm width corresponds to the region analyzed by the EC method (highlighted in purple); the magnetic measurements are carried out on a 20 mm long area (highlighted by hatching); and both the OM and EBSD analyses are carried out on a 5.5 mm long area (highlighted in green).

To obtain robust measurement using magnetic methods, a large area of the sample should be strained homogeneously. Before strain localization occurrence, the strain variation is less than 5 % within the 70 mm-long area of interest associated to uniform section, and less than 2 % within the central 20 mm, Figures 3b and 3c. Besides, DIC enables to assess strain gradient and determine the macroscopic strain level where strain localization occurs. For both RD and TD samples, necking was observed at approximately 45 % of strain.

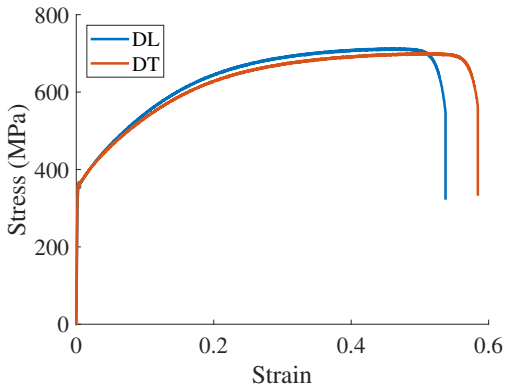

(a) Macroscopic tensile curves for RD and TD.

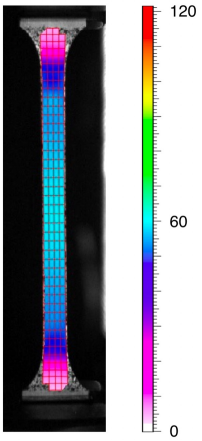

(b) DIC measurement of ε_{11}.

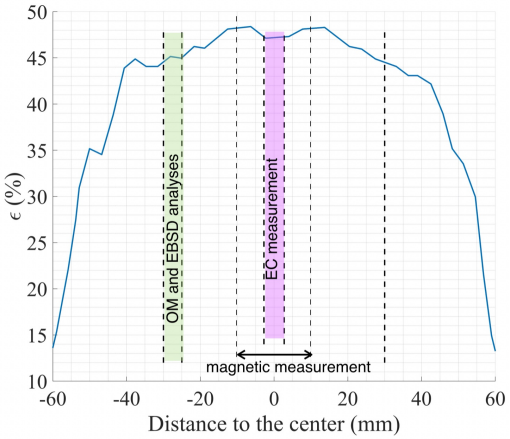

(c) Strain gradient analysis.

Figure 3: Tensile tests (a) for RD and TD specimens (b) strain field in the loading direction, and (c) strain gradient in the length of the RD specimen, corresponding to $\bar{\varepsilon} = 45$ % of macroscopic strain, colored regions of interest correspond to details in Figure 2

On this basis, interrupted tensile tests were performed in increments of 5 % of strain from 5 to 45 %. Considering both RD and TD directions, this corresponds to a total of 18 specimens. Each of them was carefully analyzed to quantify the martensitic phase transformation. Since different techniques are investigated for this quantification, the gauge length of each specimen was cut using the methods described below, after the desired strain level was reached.

3. Martensitic transformation under uniaxial loading

3.1. Sample preparation

The gauge length is 70 mm as defined above by the uniform strain. It was first cut by EDM from the whole sample, then cut into two parts: the larger one for further magnetic measurements, with a total length of 50 mm (where the magnetic measurement is carried out on 20 mm long), and the smaller one dedicated to microstructure analysis, with a total length of 5 mm (see hatched and green areas, respectively in Figure 2). This methodology implies that the microstructure is observed in an area where the strain is slightly lower than the strain reached at the center of the sample (5 %). This should be considered the maximum systematic error associated with straining the part of the specimen dedicated to microstructure analysis for both OM and EBSD, resulting in a relative error of less than 10%. This error is lower for low strain values, where strain homogeneity is higher.

3.2. Optical microscopy (OM)

For optical microscopy, Beraha etching was applied to observe phase evolution with strain, the martensitic phase being the dark phase. As shown in Figure 4, with increasing strain, a clear increase of martensitic phase is oberved, as indicated by the growing number and width of martensitic "lines".

Due to the excellent contrast between martensitic phase and the other phases in the sample, image thresholding, using ImageJ software [26], enables to quantify martensitic phase surface fraction (see Figure 5).

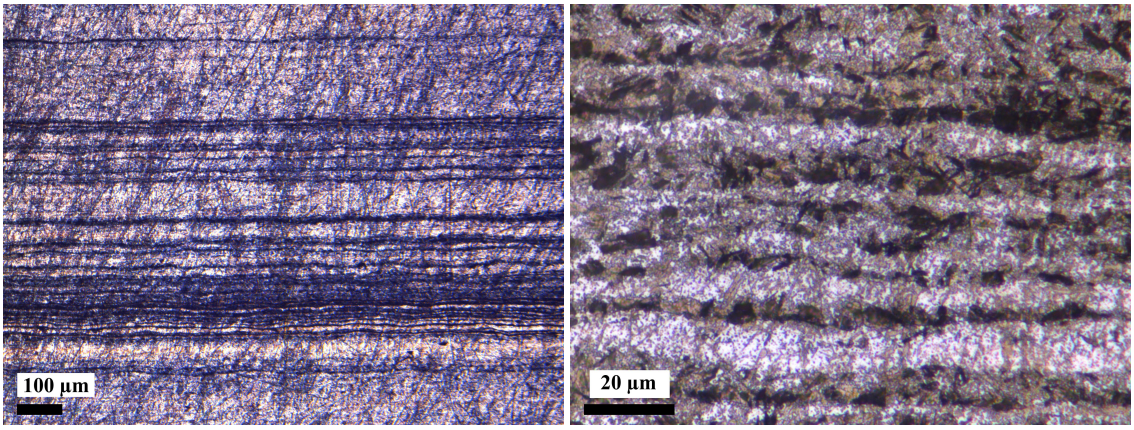

(a) ε = 25 %. (b) ε = 25 % (zoom).

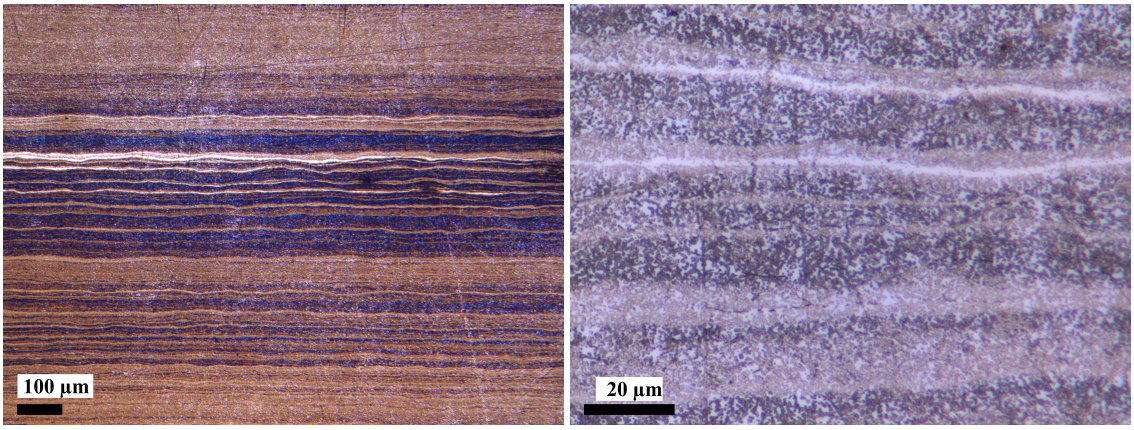

(c) ε = 35 %. (d) ε = 35 % (zoom).

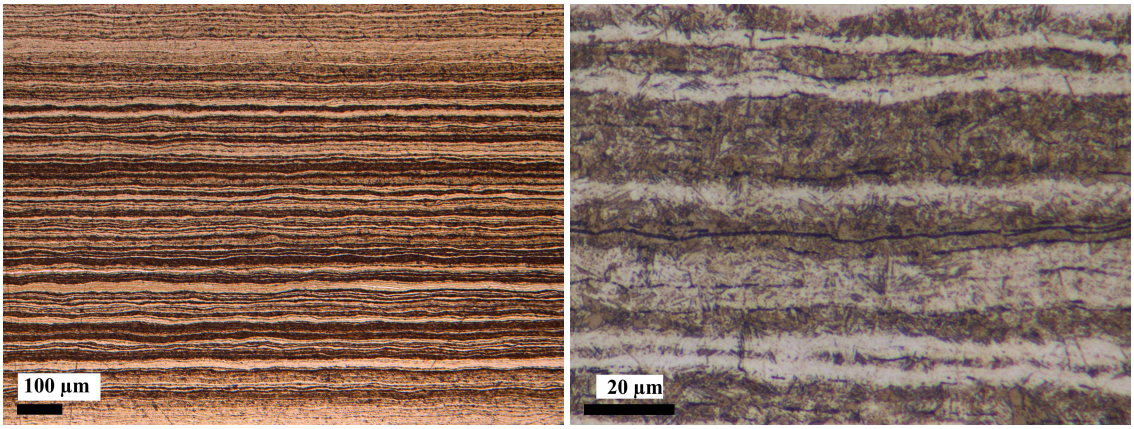

(e) ε = 45 %. (f) ε = 45 % (zoom).

Figure 4: Optical observations after Beraha etching for samples deformed at 25 %, 35 % and 45 %. RD = rolling direction, TD = transverse direction and ND = normal direction.

As a first result, we can observe that the surface fraction of martensitic phase (f_s) increases with strain, see blue square in Figure 5. Three stages are observed. Below 5 to 10 % of strain, the initiation and increase of phase

transformation are observed. The strain transformation threshold is less than 5 %. Then between 10 to 25 % of strain, a plateau on f_s is observed, reflecting a moderate martensitic transformation in the strained samples. From 25 % the martensite volume fraction is sharply increasing up to 50 % at 45 % strain.

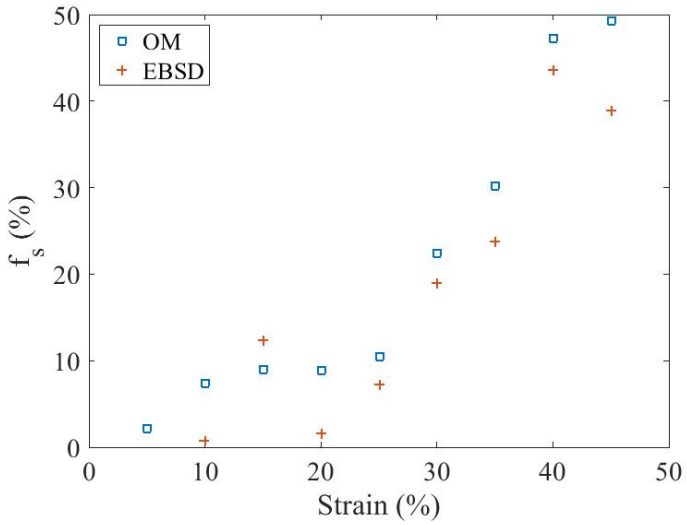

Figure 5: Martensitic phase fractions measured from optical microscopy and SEM - EBSD observations (all non austenitic phases)

3.3. EBSD Observations

To achieve more detailed microstructure analysis, EBSD measurement provides a higher spatial resolution and a validation of phases in presence based on their respective crystallographic structure: from basic austenite face centered cubic (FCC) structure, the martensitic transformation into either expected body centered cubic (BCC) martensitic phase or its quadratic form could be analyzed by EBSD, Figure 6.

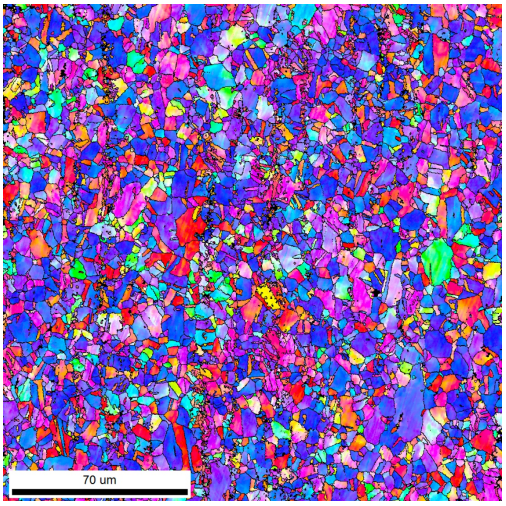

(a) IPF ($\varepsilon = 25$ %).

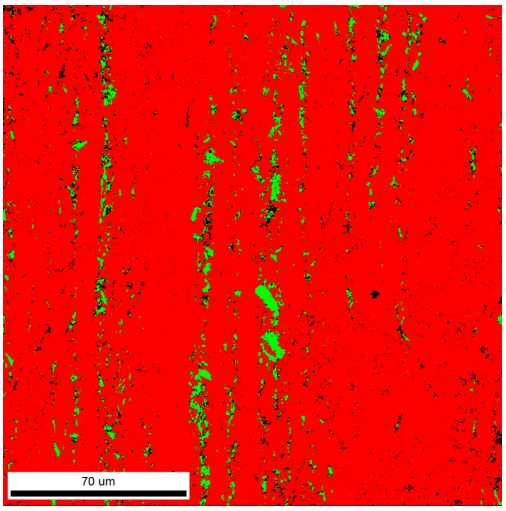

(b) Phases ($\varepsilon = 25$ %).

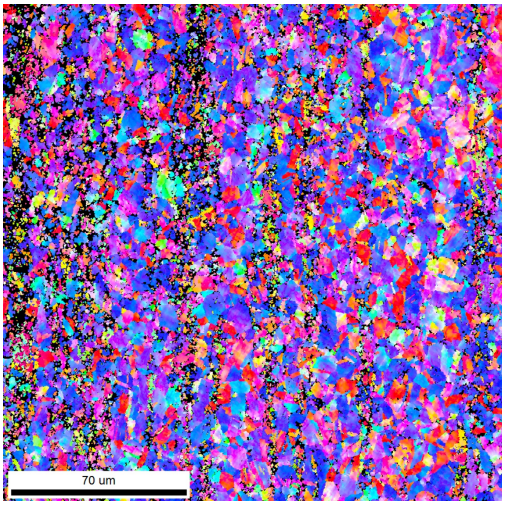

(c) IPF ($\varepsilon = 35$ %).

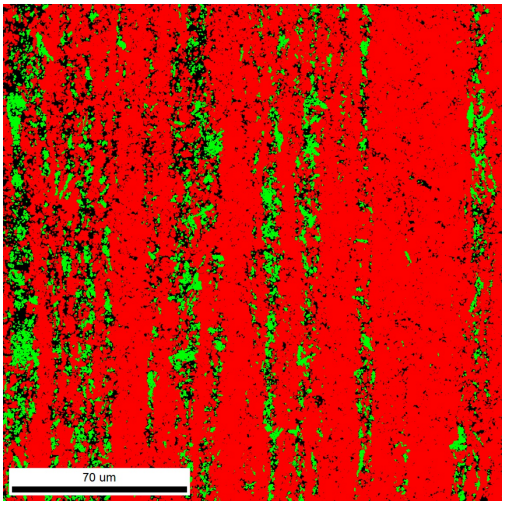

(d) Phases ($\varepsilon = 35$ %)

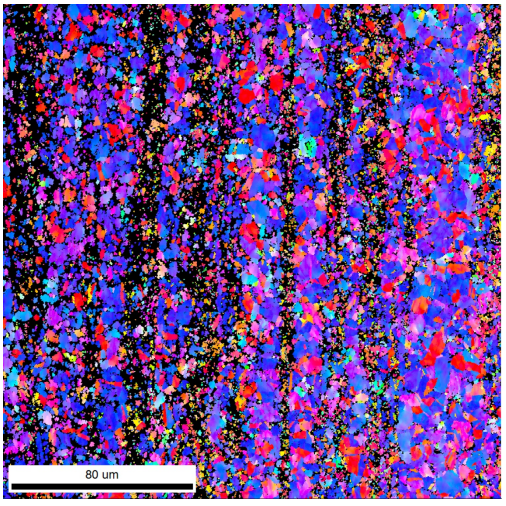

(e) IPF ($\varepsilon = 45$ %).

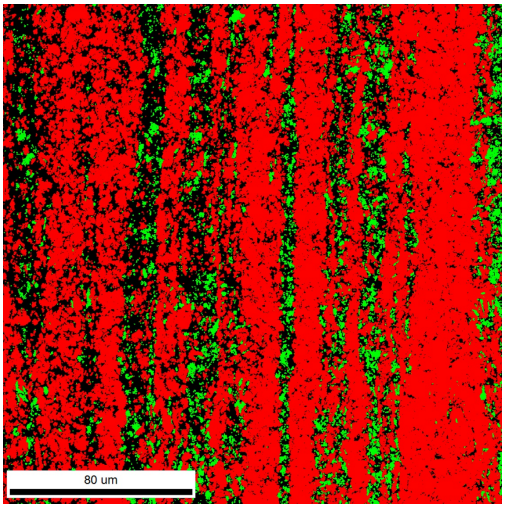

(f) Phases ($\varepsilon = 45$ %).

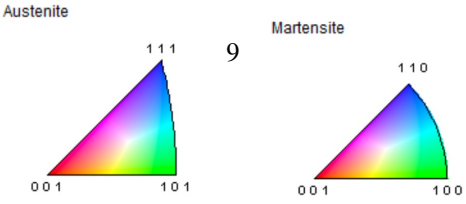

(g) Color code map for IPF.

Figure 6: Inverse pole figure (IPF) and phase volume fraction (in red austenite phase, and in green ε martensite phase) for strain levels 25 %, 35 %

As a first comparison with optical measurement, EBSD confirms that dark lines observed by OM correspond to the ε-martensite phase, whereas bright regions correspond to austenite phase. This is shown, first, by inverse pole figure (IPF) where grains sized to few microns correspond to austenite, and submicrons lines aligned with the RD direction correspond to martensite (IPF and associated zoom Figure 5). Second, a systematic identification of phases by EBSD confirms this point (phases and associated zoom Figure 5). The EBSD analysis also confirms that increasing applied strain leads to an increase in both the number and the width of the martensite "lines".

From phase measurement, it is evident that the trends highlighted by EBSD and OM are very similar (see Figure 5). Besides, some scatter and systematic error can be identified from this comparison. Firstly, in the low range of applied strain (typically below 25 %), the plateau effect is not confirmed by EBSD, and appears to be related to very low f_s values. Secondly, at higher applied strain levels, the differences between the two methods is below ± 5 %. These results support the reliability of the OM analysis in terms of resolution. However, it also raises the question of the representative volume element required to limit the scatter associated to such a local effect. It is worth noting that the region of interest used for OM measurement is of about 1 mm in width (of about 1 mm^2), whereas for EBSD measurement it is of about 150 µm (of about 0.02 mm^2). The observed scatter in EBSD measurement at low level of applied strain could be explained by the rather limited region of interest. This point will be further discussed in the sequel.

4. Indirect observation of the martensitic transformation

The tensile test series developed above provides ideal conditions for the characterization of NDT methods in two main aspects: (i) homogeneous straining and subsequent homogeneous phase transformation and (ii) large specimen size, which is particularly suitable for magnetic measurements. This section aims to establish the correlation between microhardness, magnetic permeability, and EC inductance with homogeneous strain.

4.1. Micro-hardness measurements

Microhardness measurements can provide information on the hardening of metallic alloys associated with phase transformation [27]. Here, the standard Vickers hardness (HV) analysis is applied using 0.5 kg load. HV evolves in a very continuous manner with the applied strain, Figure 7.

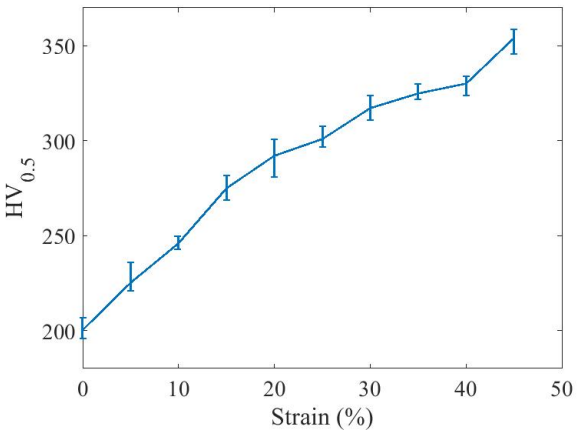

Figure 7: Evolution of the core hardness (HV) as a function of the applied strain, RD samples.

As a first result, this observation shows that HV measurements alone are not sufficient to quantify the martensitic transformation: they appear to vary monotonically with the applied strain, while previous observations have shown a strain threshold required to observe martensitic transformation and the plateau as observed in OM analysis, Figure 5.

4.2. Magnetic permeability measurements using B-coil

The magnetic behavior of the strained samples is characterized using a dedicated apparatus, presented in Figures 8a and 8b. The electromagnetic measurement consists of two U-shaped Iron-Silicon yokes ensuring the closure of the magnetic flux so as to minimize demagnetizing fields. The magnetic field is generated by two primary coils (500 turns of 20 AWG wire), powered by a power amplifier (Kepco 72-14MG). The current I is measured using a LA 125-P current transducer. The current excitation is sinusoïdal at 1 Hz frequency. The magnetic field H is measured using a GM08 Gaussmeter and a transverse Hall probe. This sensor can measure H from DC to 10 kHz with a ± 1 % accuracy. The difficulty to place the active element of the Hall probe in the same position all along the tests induces an error of ± 1 %. The measured noise level is ± 250 A.m^{-1} (one standard deviation). The electromotive force e induced in a secondary winding ($N = 60$ turns, 20 mm length) wound around the sample is evaluated in real-time. The variation of magnetic induction δB is calculated from the numerical integration of $e(t)$ based on Faraday's law. The measured noise level is evaluated at 0.2 mT, and the drift on δB always remains below 2 mT/s. The reference state for the evaluation of B is the demagnetized state. The demagnetization procedure and drift minimization techniques are detailed in [28].

The reproducibility error has been evaluated using 5 measurements per sample. This error is evaluated at 2 % (mean value, between 0.7 and 4.3 %), that is explained by the low width of the sample, and the high sensitivity of the setup to the airgap when permeability of the sample is low. The measurement acquisition, the generation of the excitation signal (including control loop feedback of the current) are ensured by a DS 1006 dSPACE processor board at a sampling frequency of 50 kHz. More details on the setup can be found in [28, 29]. Figures 8c and 8d show the magnetic behavior (two major loops for each plastic levels) obtained from RD and TD samples.

Magnetic behavior is clearly impacted by the applied strain for both RD and TD samples. The maximum induction increases with applied strain values, together with hysteresis and magnetic permeability. Because, the chosen set-up does not allow reaching saturation of the sample, we will focus on relative permeability (μ_r) analysis. This parameter is evaluated from a linear regression (10 points) of the $B(H)$ curves around $H = 0$. An average of the four values obtained for the two major loops is applied. Figure 9a shows the results obtained for RD and TD samples.

The permeability increases slightly up to 20 % strain, or could be assumed to be almost constant with $\mu_r = 1.3$. From 25 % to the maximum applied strain, the increase is drastic with $\mu_r = 5.2$ for $\varepsilon = 45$ %. This result is consistent with the evolution of the magnetization behavior observed in Figure 8. No clear difference is observed by comparing RD and TD samples considering the uncertainty of the measurements.

4.3. EC sensor measurements

The EC sensor is constituted of a circular coil covered by a ferrite ceramic disc allowing to concentrate the magnetic field created by the coil (see Figure10). The coil, containing 30 turns, has an internal diameter of 3.5 mm with an external diameter of 5.5 mm and a height of 1.2 mm. The ferrite disc has an external diameter of 6 mm with a height of 0.4 mm.

The impedance of the EC sensor is measured at 100 kHz using a Keysight E4990A impedance analyser. The spatial resolution of the EC measurement, linked to the size of the EC sensor and to the skin effect in the conductive material, is evaluated to be around 6 mm laterally and 0.5 mm in the depth [23].

The EC sensor inductance, deduced from the imaginary part of its impedance, evolves with strain in a very similar way to the magnetic permeability: it increases slightly up to 20 % strain, from 6.52 µH to 6.54 µH, Figure 9b. From 25 % to the maximum applied strain, the increase becomes more significant, reaching up to 6.85 µH. No clear difference is observed by comparing RD and TD samples considering the uncertainty of the measurements (evaluated at 16 nH), except at the maximum applied strain where the inductance measured for RD exceeds that of TD, Figure 9b.

As a partial conclusion, the above results confirm that magnetic methods, as already reported in the literature [30, 31], are good indicators of the progress of martensitic transformation. In addition, a very good correlation has been established between martensite volume fraction, magnetic permeability and EC measurement. The next step is to consider a more complex, multi-axial configuration to mimic NDT conditions.

5. Application to the detection of martensitic phase transformation under equibiaxial strain

A new experimental condition is proposed to validate the non-destructive evaluation of martensite transformation based on EC measurement. The same material is tested under equibiaxial loading using a cross-shaped specimen

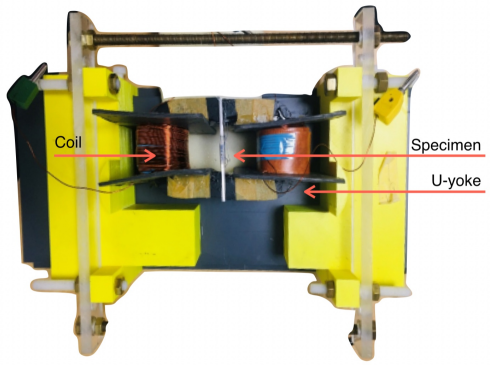

(a) Setup for magnetic characterization.

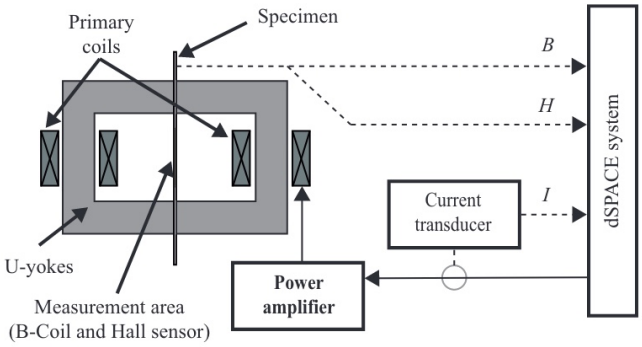

(b) Sketch of the magnetic characterization setup.

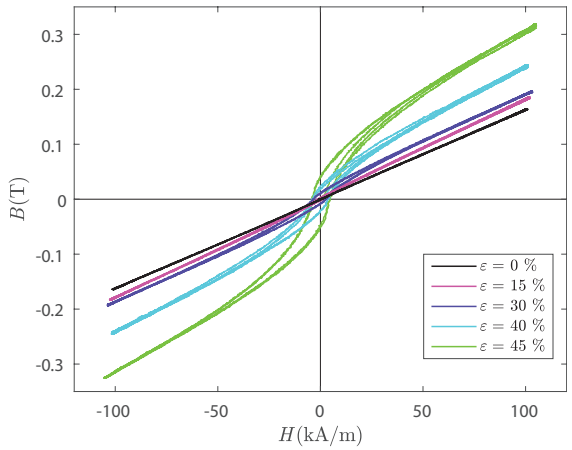

(c) RD samples.

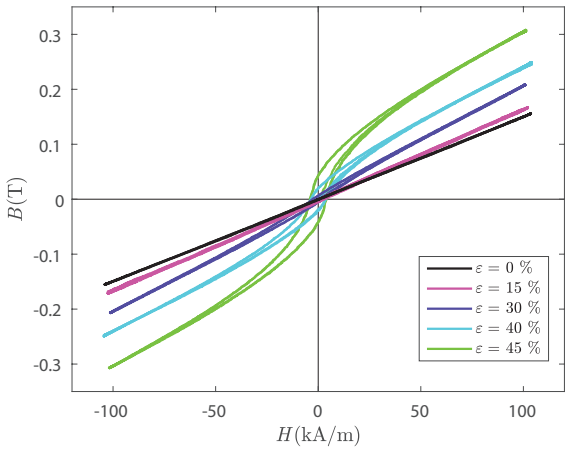

(d) TD samples.

Figure 8: Schematic of the set-up used for magnetic measurement (a,b); evolution of the magnetization curves B(H) as a function of applied strain along the RD direction (c) and TD direction (d).

with a reduced section in the middle to reach 1 mm thickness, Figure 11a. The thickness reduction in section is assymmetric, which may induce slight local bending. However, this effect is assumed here to have negligible effect on the martensitic transformation.

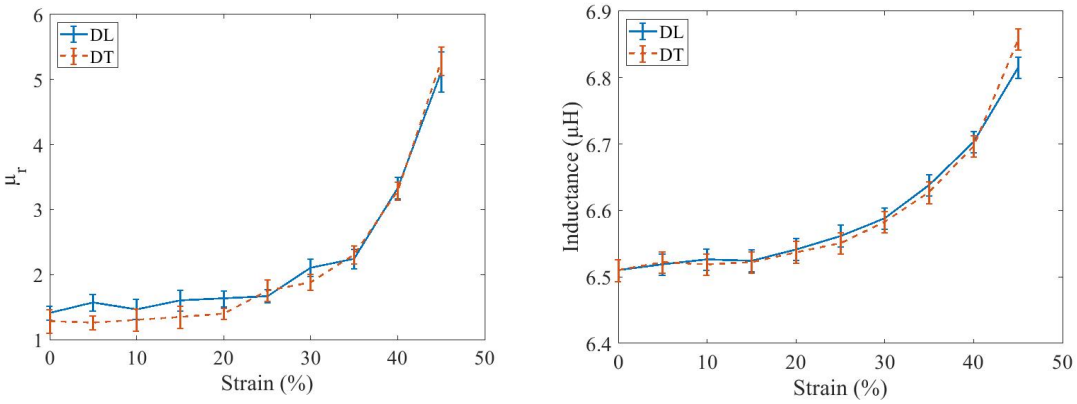

(a) Relative magnetic permeability of RD and TD samples for different values of plastic strain.

(b) EC sensor inductance at 100 kHz for RD and TD samples for different values of plastic strain.

Figure 9: Measurements of magnetic permeability (a) and EC sensor inductance (b) with strain for RD and TD samples.

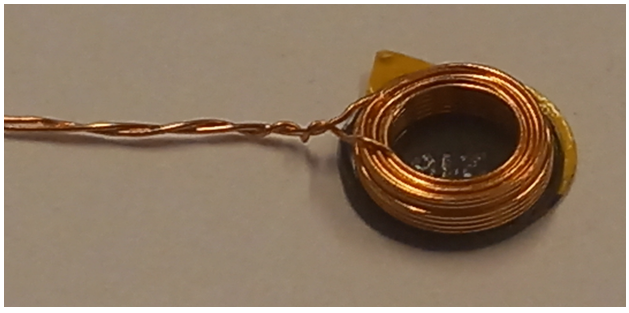

Figure 10: EC sensor.

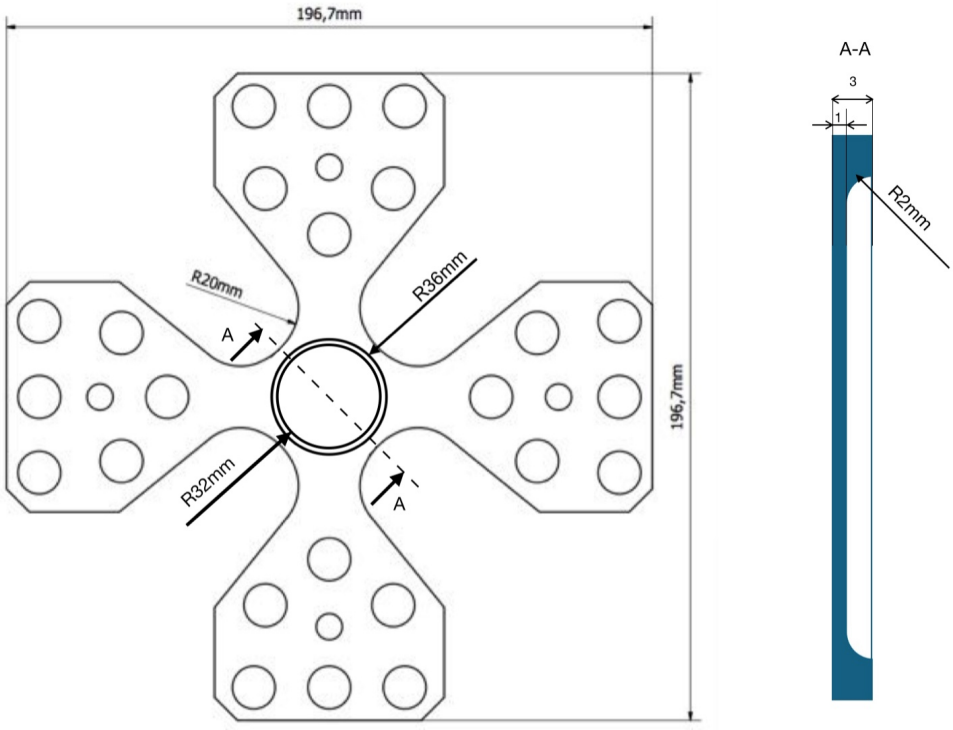

(a) Geometry of the specimen used for equibiaxial testing.

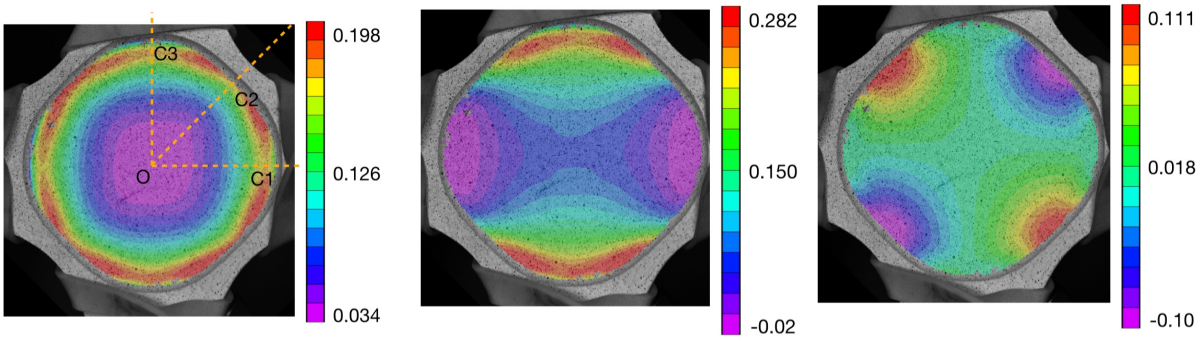

(b) ε_{eq}.

(c) ε_{yy}.

(d) ε_{xy}.

Figure 11: Details of the geometry of equibiaxial testing (a) and in situ measurement by DIC of von Mises strain ε_{eq} (b) and detail of paths analyzed by cross-sectionning (C1 corresponds to x axis and C3 to y axis respectively) ε_{yy} (c) and ε_{xy} (d).

The test facility is a coplanar device with 4 independent actuators, each with a load capacity of 100 kN. Synchronized displacements control enables the application of an equivalent von Mises strain of approximately 3 % in the central region, as shown in Figure 11b for the strain field (corresponding approximately to 2/3 of the total straining). It is worth noting that the initially circular shape of the central region deforms significantly during loading. Due to the chosen geometry, it is also observed by DIC that the strain increases with the distance from the center of the specimen, Figure 11b. Along the loading axes, the strain is close to a plane strain condition - i.e. $\varepsilon_{xx} = 0$. The maximum ε_{yy} (resp. zero) is obtained along the line C3 (resp. C1), Figure 11c. Also, the points located at 45° from the loading axis are subjected to an almost pure shear state, as shown in Figure 11d.

Due to the geometry of the sample, only the EC sensor measurements could be implemented either in situ or ex situ (i.e. sample under loading or after loading), since the fluxmetric setup is not adapted in this case. Thus, the EC measurements were performed in two ways: during the mechanical test, the impedance analyzer continuously measures the EC sensor inductance at a single point, here chosen as the center of the specimen, point O, Figure 11b; after the maximum strain was reached, the specimen was scanned ex situ through the gauge length to measure the local inductance, Figure 12a and 12b. Due to the size of the EC sensor, the analysis points are located within a central area of approximately 8 mm in radius and a spatial step of 3 mm in both x and y directions was implemented.

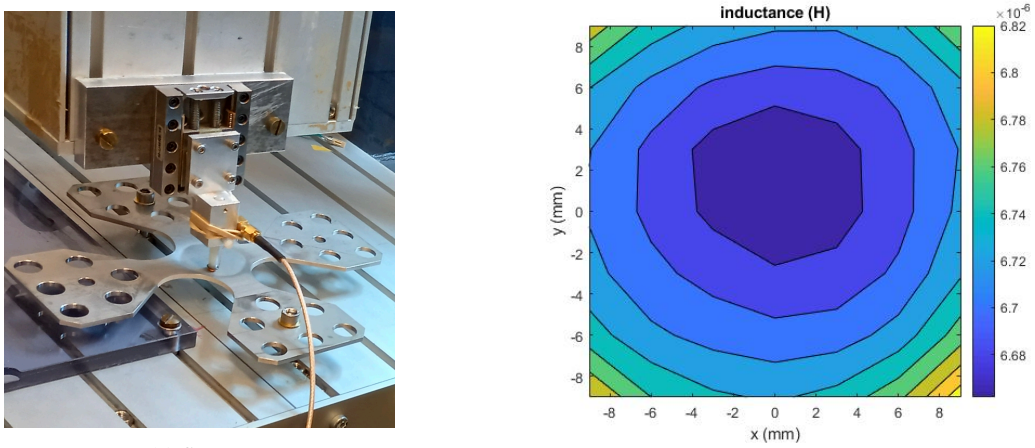

(a) Set-up.

(b) Inductance.

Figure 12: Schematic of the set-up used for EC sensor measurements ex situ (a), cartography of EC sensor inductance in the central area of the specimen (b).

The measured EC sensor inductance map reveals a strong correlation with the von Mises strain: inductance is minimal at the center of the sample and increases progressively with the distance from the center of the specimen, see Figures 11b and 12b. Assuming that the relationship between inductance and martensitic transformation observed under uniaxial loading also holds in two dimensions, the evolution of the phase transformation with applied strain in 2D can be inferred. This estimation is shown by the continuous lines labbeled "ind. cut" in Figure 13b, where the martensitic phase fraction is derived from the EC measurement using the relationship established from uniaxial tests in Figure 9b.

To validate this approach, cross-sectional samples were taken along the three paths labelled C1, C2 and C3 (dashed lines in Figure 11b), and observed using oprical microscopy (see Figure 13a). The resulting cross sections were analyzed using the same etching and image analysis procedure as for the uniaxial tests, in order to estimate the surface fraction of martensite.

As a first result, it is observed that despite careful etching conditions, the image analysis is very noisy, yielding a systematic error of about 10 %, Figure 13b. This uncertainty arises from two factors. First, martensitic transformation is a localized phenomenon, often appearing in "bands" of martensitic structure, which may be influenced by the rolling of the material. This has also been observed in uniaxial tests, Figure 5. Second, the etching is heterogeneous along

the cross section, which likely contributes substantially to the variability in the measurements.

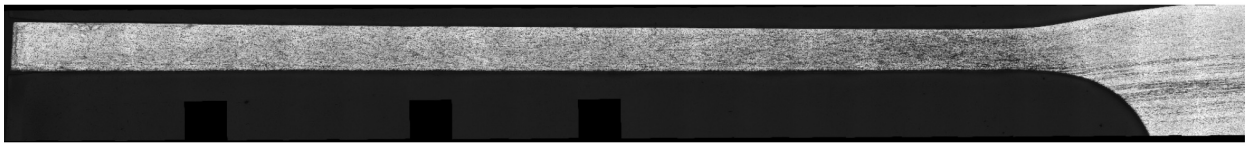

(a) Cross-section C1 observed by OM.

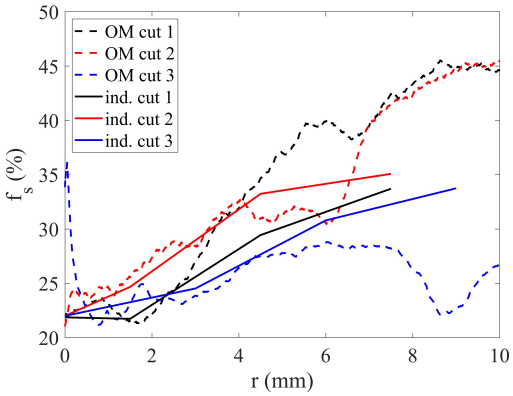

(b) Martensite fraction on different cuts from OM (dashed lines) and from EC sensor measurement (continuous lines).

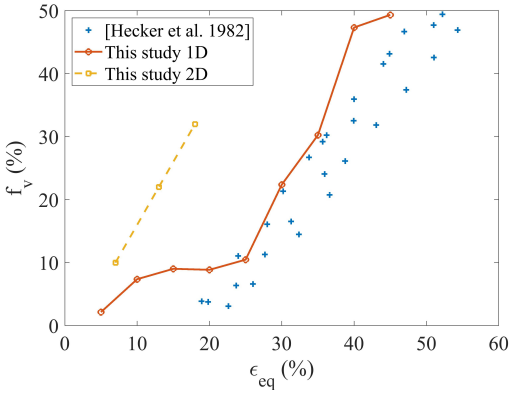

(c) OM results compared to literature data.

Figure 13: Martensitic phase transformation from equibiaxial loading, measured by OM, EC sensor measurement and comparison to results from [4].

However, on the three cross-sections and paths C1 to C3, a clear correlation is obtained between the fraction of martensite measured by analyzing the cross-section and that measured by the EC technique (see Figure 13b). Despite the relatively high noise to signal ratio, this provides some confidence in the proposed method of EC sensor measurements. OM analysis may have been improved to limit scatter, but this is not the intent of the proposed study to have a detailed quantification of this effect.

Based on our estimate of martensite volume fraction obtained from EC NDT, we compare these results with others from the literature, by plotting the martensite volume fraction as a function of the von Mises equivalent strain, denoted as ε_{eq}, see Figure 13c. While our results agree well with Hecker *et al.* [4] for uniaxial tension, they show that, contrary to the statement in [4], the von Mises equivalent strain may not be a good indicator of phase transformation. This could be an effect of a competition between different variants of phase transformation as observed by [10]. It also shows the extreme sensitivity to local loading, which in our case is measured by DIC, whereas Hecker *et al.* used a grid method without any detail regarding the spatial resolution of the set-up. Last but not least, Hecker *et al.* used a flat-punch set-up, which may greatly increase bending effect, mitigating the influence of multiaxial loading.

Finally, the proposed equibiaxial test demonstrates the potential of local measurements combining EC sensor and DIC.

6. Conclusions

The proposed study deals with the non-destructive evaluation of the stress induced phase transformation from austenite to martensite in the stainless steel A304L. The methodology is based on the comparison of different techniques: direct observation of the phase transformation by microstructural analysis based on OM and EBSD measurements, and indirect analysis by microhardness, magnetic permeability and EC sensor measurements. The use of these

methods for NDT purposes is encouraged by the linearity of both permeability and EC sensor inductance as a function of phase transformation. The relationship between microhardness and phase transformation is less straightforward because microhardness is continuously affected by the hardening of the material.

As a validation step, an equibiaxial test was analyzed using EC sensor measurements and the local strain field. The ability of the local EC measurement to assess phase transformation was confirmed. This final test also raised questions about the OM and etching technique for accurate quantification of the martensitic phase transformation. Indeed, a large volume of material is required to assess a representative phase transformation due to the high heterogeneity of the transformation. Finally, this study paves the way for the use of EC measurement as an NDT technique, taking advantage of the small size of the sensor, which could be applied to complex geometries.

Declarations

Ethical Approval

not applicable

Funding

This work did not received any grant.

Availability of data and materials

Data will be available on request

[1] B. J. Tuazon, N. A. V. Custodio, R. B. Basuel, L. A. Delos Reyes, J. R. C. Dizon, 3d printing technology and materials for automotive application: a mini-review, Key Engineering Materials 913 (2022) 3–16.

[2] M. Rezayat, M. Karamimoghadam, M. Moradi, G. Casalino, J. J. Roa Rovira, A. Mateo, Overview of surface modification strategies for improving the properties of metastable austenitic stainless steels, Metals 13 (7) (2023) 1268.

[3] Y. Guanghua, H. Xinmin, W. Yanqing, Q. Xingguo, Y. Ming, C. Zuoming, J. Kang, Effects of heat treatment on mechanical properties of h13 steel, Metal Science and Heat Treatment 52 (2010) 393–395.

[4] S. Hecker, M. Stout, K. Staudhammer, J. Smith, Effects of strain state and strain rate on deformation-induced transformation in 304 stainless steel: Part i. magnetic measurements and mechanical behavior, Metallurgical Transactions A 13 (1982) 619–626.

[5] L. Murr, K. Staudhammer, S. Hecker, Effects of strain state and strain rate on deformation-induced transformation in 304 stainless steel: Part ii. microstructural study, Metallurgical Transactions A 13 (1982) 627–635.

[6] H. C. Shin, T. K. Ha, W. J. Park, Y. W. Chang, Deformation-induced martensitic transformation under various deformation modes, Key Engineering Materials 233 (2002) 667–672.

[7] S. Nanga, A. Pineau, P.-O. Santacreu, B. Tanguy, Strain induced martensitic transformations in two austenitic stainless steels: macro-micro behaviour, in: ECF 17, 2008, pp. 1373–1380.

[8] S. Nanga-Nyongha, Comportement et transformations martensitiques de deux aciers inoxydables austénitiques : effets de la température, de la vitesse et du chargement (in French), Theses, École Nationale Supérieure des Mines de Paris (Nov. 2008).
URL https://pastel.hal.science/pastel-00577815

[9] A. M. Beese, D. Mohr, Effect of stress triaxiality and lode angle on the kinetics of strain-induced austenite-to-martensite transformation, Acta Materialia 59 (7) (2011) 2589–2600.

[10] E. Polatidis, M. Šmíd, W.-N. Hsu, M. Kubenova, J. Capek, T. Panzner, H. Van Swygenhoven, The interplay between deformation mechanisms in austenitic 304 steel during uniaxial and equibiaxial loading, Materials Science and Engineering: A 764 (2019) 138222.

[11] E. Polatidis, G. Haidemenopoulos, D. Krizan, N. Aravas, T. Panzner, M. Šmíd, I. Papadioti, N. Casati, S. Van Petegem, H. Van Swygenhoven, The effect of stress triaxiality on the phase transformation in transformation induced plasticity steels: Experimental investigation and modelling the transformation kinetics, Materials Science and Engineering: A 800 (2021) 140321.

[12] V. Shrinivas, S. Varma, L. Murr, Deformation-induced martensitic characteristics in 304 and 316 stainless steels during room-temperature rolling, Metallurgical and Materials Transactions A 26 (1995) 661–671.

[13] J. Talonen, H. Hänninen, Formation of shear bands and strain-induced martensite during plastic deformation of metastable austenitic stainless steels, Acta materialia 55 (18) (2007) 6108–6118.

[14] Y. Shen, X. Li, X. Sun, Y. Wang, L. Zuo, Twinning and martensite in a 304 austenitic stainless steel, Materials Science and Engineering: A 552 (2012) 514–522.

[15] E. Polatidis, M. Morgano, F. Malamud, M. Bacak, T. Panzner, H. Van Swygenhoven, M. Strobl, Neutron diffraction and diffraction contrast imaging for mapping the trip effect under load path change, Materials 13 (6) (2020) 1450.

[16] S. Rawat, S. P. Joshi, Effect of multiaxial loading on evolution of $\{101\ 2\}$ twinning in magnesium single crystals, Materials Science and Engineering: A 659 (2016) 256–269.

[17] I. Janeiro, O. Hubert, J.-H. Schmitt, In-situ strain induced martensitic transformation measurement and consequences for the modeling of medium mn stainless steels mechanical behavior, International Journal of Plasticity 154 (2022) 103248.

[18] S. Tavares, D. Fruchart, S. Miraglia, D. Laborie, Magnetic properties of an aisi 420 martensitic stainless steel, Journal of alloys and compounds 312 (1-2) (2000) 307–314.

[19] J. Talonen, P. Aspegren, H. Hänninen, Comparison of different methods for measuring strain induced α-martensite content in austenitic steels, Materials Science and Technology 20 (12) (2004) 1506–1512.
[20] A. Beese, D. Mohr, Identification of the direction-dependency of the martensitic transformation in stainless steel using in situ magnetic permeability measurements, Experimental mechanics 51 (2011) 667–676.
[21] M. Shirdel, H. Mirzadeh, M. Parsa, Estimation of the kinetics of martensitic transformation in austenitic stainless steels by conventional and novel approaches, Materials Science and Engineering: A 624 (2015) 256–260.
[22] N. Leuning, M. Heller, M. Jaeger, S. Korte-Kerzel, K. Hameyer, A new approach to measure fundamental microstructural influences on the magnetic properties of electrical steel using a miniaturized single sheet tester, Journal of Magnetism and Magnetic Materials 583 (2023) 171000.
[23] J. Blitz, Electrical and magnetic methods of non-destructive testing, Vol. 3, Springer Science & Business Media, 1997.
[24] C. Hellier, et al., Handbook of nondestructive evaluation, Tech. rep., Mcgraw-hill (2003).
[25] M. A. Sutton, J. J. Orteu, H. Schreier, Image correlation for shape, motion and deformation measurements: basic concepts, theory and applications, Springer Science & Business Media, 2009.
[26] ImageJ, Image processing and analysis in java, v1.43s, http://rsbweb.nih.gov/ij/.
[27] C. Hayzelden, B. Cantor, The martensite transformation in fe-ni-c alloys, Acta Metallurgica 34 (2) (1986) 233–242.
[28] M. Domenjoud, E. Berthelot, N. Galopin, R. Corcolle, Y. Bernard, L. Daniel, Characterization of giant magnetostrictive materials under static stress: influence of loading boundary conditions, Smart Materials and Structures 28 (9) (2019) 095012.
[29] M. Domenjoud, L. Daniel, Effects of plastic strain and reloading stress on the magneto-mechanical behavior of electrical steels: Experiments and modeling, Mechanics of Materials 176 (2023) 104510.
[30] K. Mumtaz, S. Takahashi, J. Echigoya, Y. Kamada, L. Zhang, H. Kikuchi, K. Ara, M. Sato, Magnetic measurements of martensitic transformation in austenitic stainless steel after room temperature rolling, Journal of Materials Science 39 (2004) 85–97.
[31] I. Mészáros, J. Prohászka, Magnetic investigation of the effect of α'-martensite on the properties of austenitic stainless steel, Journal of Materials Processing Technology 161 (1-2) (2005) 162–168.